Energy 307 (2024) 132514

Contents lists available at ScienceDirect

Energy

journal homepage: www.elsevier.com/locate/energy

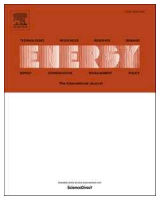

Experimental study of electricity generation from solar energy using organic phase change materials and thermoelectric generator

Ali Mortazavi [a], Emadoddin Erfani Farsi Eidgah [a], Mohammad Mustafa Ghafurian [a,b,**], Saleh S. Meibodi [c], Ali Kianifar [a,*], Ahmad Arabkoohsar [b]

[a] Department of Mechanical Engineering, Ferdowsi University of Mashhad, Mashhad, Iran
[b] Department of Civil and Mechanical Engineering, Thermal Energy Section, Technical University of Denmark, Kgs. Lyngby, Denmark
[c] School of Computing, Engineering & Digital Technologies, Teesside University, Middlesbrough, TS1 3BX, UK

ARTICLE INFO

Keywords:
Thermal energy storage
Phase change materials
Nanoparticles
Carbonized sawdust

ABSTRACT

The study investigates using edible oils (ostrich, mutton, beef, coconut) as natural phase change materials for solar energy absorption and storage. Exposed to 900 W/m^2 direct radiation by a solar simulator, these materials harness captured energy at a specific depth to generate electricity through a thermoelectric device. The experimental results showed that coconut oil exhibits the highest thermal energy storage efficiency among others, measuring at 39 %, while mutton tallow shows the lowest performance at 16.59 %. Additionally, the performance of a system employing coconut oil as the best material, in combination with iron oxide nanoparticles and carbonized sawdust (CS) was experimentally evaluated at different mass fractions (0.3 %, 0.6 %, and 0.9 %) to enhance thermal conductivity and sunlight absorption. The carbonized sawdust and its nanoparticles increased the thermal energy storage efficiency of the system by 62 % and 53 %, respectively. Moreover, the stored exergy by the phase change materials indicates that coconut oil and beef tallow had the highest and lowest exergy efficiencies of 6.3 % and 3.3 %, respectively. The combination of coconut oil with iron oxide nanoparticles and carbonized sawdust leads to 10 % and 7.9 % increased exergy efficiencies respectively.

Nomenclature

A	Area [m^2]
C_p	Specific heat capacity [J/(g k)]
I	Solar radiation flux [kW/m^2]
k	Thermal conductivity [W/(m k)]
m	Mass [g]
Q_s	Heat energy stored [J]
T	Temperature [°C]
t	Time [s]
Greeks	
∅	Volume fraction
η	Efficiency
Ψ	Exergy
Acronyms	
CS	Carbonized sawdust
DSC	Differential Scanning Calorimeter
PCM	Phase change materials
SEM	Scanning electron microscopy
TEG	Thermoelectric generator

(*continued on next column*)

(*continued*)

Subscripts	
a	Two-phase region
amb	Ambient
c	Cold sides of the thermoelectric generator
Co	Coconut oil
ex	Exergy
fin	Final
h	Hot sides of the thermoelectric generator
ini	Initial
l	Liquid phase
Nano	Iron oxide nanoparticles
s	Solid phase

1. Introduction

The current state of energy demand and supply is unsustainable in terms of its environmental, social, and economic impacts. The increasing

** Corresponding author. Department of Mechanical Engineering, Ferdowsi University of Mashhad, Mashhad, Iran.
* Corresponding author. Department of Mechanical Engineering, Ferdowsi University of Mashhad, Mashhad, Iran.
E-mail addresses: emad.efy@gmail.com (E. Erfani Farsi Eidgah), mmugh@dtu.dk (M.M. Ghafurian), a-kiani@um.ac.ir (A. Kianifar).

https://doi.org/10.1016/j.energy.2024.132514
Received 11 November 2023; Received in revised form 30 May 2024; Accepted 18 July 2024
Available online 19 July 2024

rate of fossil fuel consumption has raised concerns about energy resources. It is predicted that with a 119 % increase in extraction from fossil fuel sources from 2015 to 2050, greenhouse gas emissions also increase by approximately 41 % [1]. Therefore, reducing the consumption of fossil fuels and focusing on sustainable and renewable energy sources such as solar, wind, biomass, hydrogen, and geothermal energy is deemed necessary [2,3]. Solar energy is regarded as one of the most promising renewable energy sources, given its high accessibility and affordability [4–6]. Among various clean technologies, solar thermal systems have gained significant recognition as practical and highly effective measures of sustainable heat supply for a wide range of applications including electricity generation, steam production for industrial processes, domestic hot water generation, etc. However, the intermittent and unstable nature of solar radiation poses a challenge to its direct and continuous utilization [7]. Therefore, heat storage systems can significantly enhance their applicability and ensure a consistent supply of energy. Thermal energy storage solutions come in three classes: sensible, latent, and thermochemical heat storage [8,9].

Phase change materials (PCMs), in the category of latent heat storage, are substances capable of absorbing and releasing considerable amounts of heat during phase transitions, making them ideal for solar thermal systems [10]. Irani et al. [11] evaluated the effect of a paraffin wax as a PCM on the performance of the direct surface and volumetric solar steam generation systems. The results showed that the presence of paraffin can effectively reduce the evaporation rate during solar radiation. However, when the radiation is interrupted, the PCM tends to increase the evaporation rate to some extent. Sui et al. [12] conducted an experimental investigation on the utilization of paraffin with two different melting points in a concentration solar Thermoelectric Generator (TEG) unit, for thermal energy storage and power conversion. In their study, they utilized a heat sink for cooling the TEG and transferring heat to the PCM. The findings revealed that an increase in the concentration ratio of solar radiation led to higher thermoelectric efficiency of the unit but at a decreasing rate. Additionally, altering the height of the heat sink was found to have a notable impact on energy storage capacity and voltage generation. Maleki et al. [13] conducted an empirical comparison between two systems consisting of a solar cell and a TEG accompanied by paraffin at two different melting temperatures, as well as a system without PCMs. Their results demonstrated that the system incorporating PCMs could reduce the average temperature of the solar cell by 89.4 % and increase the temperature gradient of the thermoelectric device by 1.2 %. The average electrical efficiency with PCMs was 8.1 % higher than of without PCMs.

Pure PCMs have low thermal conductivity, resulting in reduced energy storage capacity and efficiency. As a result, adding highly conductive materials to the PCM (e.g. carbon materials, metal oxides, nanoparticles, and graphene) can be a good approach for addressing this shortcoming [14–16]. Luo et al. [17] evaluated the performance of a novel solar TEG using evacuated tubular solar collectors and a composite of expanded graphite (EG) and paraffin with four distinct melting temperatures. They found that paraffin with a higher melting temperature can store a greater amount of energy. They also indicated the paraffin/EG composite not only addresses the low thermal conductivity issue but also resolves the problem of liquid paraffin leakage. Nourani et al. [18] experimentally investigated the thermal behaviour of aluminium oxide nanoparticles in paraffin. They demonstrated that the addition of the aluminium oxide nanoparticles into paraffin exhibited favourable thermal reliability, boosting thermal conductivity by up to 31 % and increasing the melting rate by 27 %. Zhang et al. [19] investigated the composite of copper foam as a base, and reduced graphene oxide as surface modifiers in paraffin and polyethene glycol. Their results demonstrated that the thermal conductivity was increased by 300 % and 124 %, respectively, by the copper oxide-graphene oxide composite and reduced graphene oxide composite in paraffin and polyethene glycol. The photothermal conversion efficiency of paraffin and polyethene glycol reached 86.7 % and 78.8 % respectively. Chen et al. [20] examined the composite of copper oxide nanoparticles and paraffin for solar thermal conversion, heat storage, and thermoelectric applications. They found that the addition of copper oxide nanoparticles to paraffin enhanced the PCM performance and improved solar thermal capacity. Furthermore, in solar thermoelectric experiments, the open-circuit voltage of the copper oxide nanoparticle-paraffin composite was 1.8 times higher than that of pure paraffin, and the composite exhibited the ability to generate voltage even when the solar simulator was off. Shi et al. [21] studied the use of paraffin with added magnetic nanoparticles as a magnetic PCM for solar thermal applications. It was found that increasing the magnetic field strength led to an improvement of over 48 % in storage capacity, efficiency, and open-circuit voltage. Cao et al. [22] evaluated the effect of PCM methyl palmitate on the voltage changes of a thermoelectric module. Their results showed that using the thermoelectric module along with the PCM increases the temperature difference by 2.8 times on both sides of the thermoelectric compared to a regular thermoelectric. This PCM caused the output voltage of the thermoelectric to be 9 times higher than a regular thermoelectric.

Many PCMs, including paraffin, are derived from petroleum, a non-renewable resource which is considered an indirect contributor to global warming [23]. For this reason, researchers have been actively exploring more environmentally friendly alternatives. One of the alternatives is to utilize natural PCMs which are derived from renewable and environmentally friendly sources, such as agricultural products, and food materials. Examples of such materials include date seed oil, palm oil, coconut oil, soybean oil, and animal fats [24]. For instance, Thaib et al. [25] examined the thermal properties of cow fat and coconut oil as organic PCMs. They reported the combination of cow fat with coconut oil resulting in a decrease in the melting temperature, latent heat, and specific heat capacity compared to cow fat alone. Jurčević et al. [26] conducted an experimental study on hybrid PCMs which were composed of pork fat as the base PCM along with waste burnt oil and sunflower oil. The findings of the study demonstrated that the best hybrid PCM was a combination of pork fat and waste burnt oil, resulting in an enhanced thermal conductivity by 1.4 %. Kahwaji et al. [27] investigated edible oils as PCMs including margarine, vegetable shortening, and coconut oil for thermal energy storage. They identified coconut oil, due to its relatively higher heat capacity compared to margarine and vegetable shortening, as a superior PCM for thermal energy storage. Liu et al. [28] proposed a ternary PCM gel (PCMGs) comprising octadecanol (based on coconut oil), styrene-ethylene-butylene-styrene, and hydroxylated carbon nanotubes for biomass utilization, aiming to harness solar energy for storage and conversion into electricity. The proposed biomass-based PCM gels exhibited a thermal energy storage capacity of approximately 183 J/g and a solar absorbance of 96 %. Table 1 presents previous research studies on the applications of PCMs in solar energy absorption, storage, and conversion into electricity. As seen, paraffin wax is a commonly used PCM in solar power systems due to its high latent heat and cost-effectiveness. It demonstrates a high thermal capacity over 400 phase change cycles, in addition to improving energy efficiency [29]. Nanoparticles have been utilized to enhance the thermal performance of PCMs. However, according to previous studies reviewed, the potential of using inexpensive and readily available edible oils, especially when combined with nanoparticles, is evident. Therefore, the present study focuses on the experimental investigation of absorption, storage, and conversion of solar energy into electricity using environmentally friendly and economically viable organic PCMs. These edible PCMs are used not only for cooling photovoltaic panels but also in various solar systems such as solar heating devices [30], solar absorption cooling systems [31], solar dryers [32], and solar cookers [33]. In this study, edible PCMs such as mutton tallow, beef tallow, ostrich oil, and coconut oil (due to their suitable thermophysical properties such as high storage density, appropriate phase change temperature and high durability [34–36]) are primarily utilized for solar thermal energy storage, which is rarely investigated in previous research studies. Then, iron oxide

Table 1
Summary of previous research on the application of PCMs in energy storage and generation.

System	Findings	PCM	Additives	Irradiance (kW/m^2)	Max. Power generation (mV)	Max. Energy storage efficiency (%)	Ref.
The water container surrounded by a PCM under radiation.	In the absence of radiation, the evaporation rate increased by 45 % using a PCM.	Paraffin	–	1.2	–	–	[11]
Using a Fresnel lens to focus radiation onto one side of a thermoelectric device, while the other side of the thermoelectric device is connected to a heat sink inside the PCM container.	The use of a Fresnel lens and varying the height of the heat sink has a significant impact on energy storage and electricity generation. The heat sink, with long, medium, and short heights, produced average voltages of 1.025, 0.4204, and 0.299 V, respectively.	Paraffin with two different melting temperatures, 35 and 56 °C.	–	0.9	700	–	[12]
Photovoltaic system.	The presence of a PCM reduced the average temperature of the solar cell by 4.89 %. Additionally, it increased the temperature gradient of the thermoelectric material by 1.2 %.	paraffin with two distinct melting temperatures (32 °C and 45 °C (	–	1.156	450	50.2	[13]
Using a vacuum tube for energy absorption.	In the absence of irradiation, the PCM with a higher melting point generated a higher voltage. Additionally, during solar irradiation, the sample containing expanded graphite in paraffin with a higher melting temperature produced electricity of 2.697 V.	Paraffin with different melting temperatures, 50,60,70 and 80 °C.	Expanded graphite with a mass ratio of 3:7.	1	1500	–	[17]
A type K thermometer was placed at the center of a test tube to measure temperature changes throughout the experiment.	For the sample containing 10 % by weight fraction of aluminum oxide nanoparticles, the melting rate increased by 27 %.	Paraffin	Aluminum oxide nanoparticles with a mass fraction ranging between 0 and 10 %	–	–	–	[18]
The container of the PCM exposed to a solar simulator that simulates sunlight, and its temperature is recorded by a data logger.	The thermal conductivity of composites containing copper oxide, graphene oxide, and reduced graphene oxide has decreased when individually dispersed in paraffin and polyethylene glycol 10000 by 300 % and 124 %, respectively. Furthermore, the thermal efficiency of paraffin and polyethylene glycol 10000 reached 86.68 % and 78.79 % respectively.	Paraffin and polyethylene glycol (PEG 10000)	2 mg of copper foam, reduced graphene oxide, and reduced graphene oxide with a volume fraction of 5 %.	1	–	–	[19]
The container of the PCMs placed on the thermoelectric module, while the other side of the module is connected to a heat sink.	By increasing the concentration of copper oxide nanoparticles to 0.1 % by weight, after 30 min of irradiation, the maximum temperature and voltage increased by a factor of 2/3 and 1/8, respectively.	Paraffin	Copper oxide nanoparticles with a mass fraction of 0–0.1 %	10	1350	90	[20]
The PCM container positioned on the thermoelectric module, while the heat sink is placed alongside it	The temperature of paraffin in the presence of nanoparticles increases more rapidly compared to pure paraffin, and it also reaches a higher maximum temperature. Furthermore, by placing a PCM container in a magnetic field of 200 mT, energy storage is enhanced by 48 %, and voltage generation is increased by 50 %.	Paraffin	Fe_3O_4/CNTs nanoparticles with a mass fraction of 0–6%.	7	2500	91	[21]
A PCM is placed inside the heat source and is exposed to radiation. A thermoelectric module is located beneath the heat source, and underneath the thermoelectric module, a water cooler is installed for forced cooling.	The presence of the PCM led to a 2.8-fold increase in the temperature difference across thermoelectric compared to a conventional thermoelectric. Additionally, this PCM caused the output voltage of the thermoelectric to be 9 times	methyl palmitate	_	1	307	_	[22]

(*continued on next page*)

Table 1 (*continued*)

System	Findings	PCM	Additives	Irradiance (kW/m^2)	Max. Power generation (mV)	Max. Energy storage efficiency (%)	Ref.
	greater than that of a conventional thermoelectric.						
A setup consisting of two tubes, one filled with a PCM and the other containing water (as a reference), along with a heated water container, has been employed for the purposes of PCM melting and water heating.	The combination of these PCMs with each other results in a reduction in melting temperature, latent heat, and specific heat capacity compared to bovine fat oil.	Mixing beef fat with coconut oil.	The combination of PCMs with each other.	–	–	–	[25]
The Hot Disk TPS 500 S device is utilized for measuring thermal conductivity.	The addition of waste oils to pork fat resulted in an increase in volumetric heat capacity and thermal conductivity.	Pork fat, waste cooking oils and industrial oils.	Combining pork fat with waste cooking oils and industrial oils.	–	–	–	[26]
The Differential Scanning Calorimetry (DSC)	Coconut oil exhibited a higher specific heat capacity compared to margarine. Additionally, when analyzing the energy storage capacity of coconut oil and water, coconut oil demonstrated three times higher energy storage than water.	Coconut oil and margarine	–	–	–	–	[27]
The system consists of a heat sink and a thermoelectric element, where the PCM is placed on the thermoelectric element. Additionally, the heat sink is utilized to dissipate heat below the thermoelectric element.	The triple-component PCM gel demonstrated a substantial energy storage capacity of approximately 183 J/g. Furthermore, incorporating carbon nanotubes at a mass fraction of 0.7 % resulted in a sixfold increase in voltage generation compared to the absence of carbon nanotubes.	PCMG comprising octadecanol based on coconut oil	Combining hydroxylated carbon nanotubes with a mass fraction range of 0–0.7 %.	3	300	–	[28]

nanoparticles are added to enhance the thermal behaviour of the PCMs. Considering the high cost of nanoparticles, carbonized sawdust (CS) will be separately utilized as a plentiful and cost-effective alternative to enhance solar energy absorption and storage. Ultimately, the performance of organic PCMs using nanoparticles and carbonized sawdust is compared in terms of energy storage capacity/efficiency, exergy efficiency, and electricity generation rate. The innovations of this research can be summarized as follows:

- The utilization of organic, renewable, inexpensive, and easily accessible oils as PCMs for harvesting and storing solar energy and determining the most competent materials among all,
- Investigating the effect of using carbonized sawdust as an abundant and affordable material to enhance sunlight absorption and comparing it with the effect of adding Fe_3O_4 nanoparticles.
- Experimental assessment of the proposed method for measuring the energy and exergy efficiencies, and electricity generation potential, for the combinations of the best PCM with carbonized sawdust and iron oxide nanoparticles.

2. Experimental setup and operation description

The laboratory setup used in this research consists of a PCM chamber, a thermoelectric module, and a heat sink, as shown in Fig. 1. In this system, a solar simulator with a 1000-W Xenon lamp is utilized as an artificial sunlight source. The glass chamber serves as a sunlight absorber, with dimensions of 40 mm × 35 mm, a height of 38 mm, and a thickness of 2 mm, containing the PCMs. Greater volume generally increases the time required to reach the phase change point because energy must transfer through more material. Conversely, shallower depths can result in faster energy absorption and quicker phase change, which lead to increased thermal losses to the environment. Therefore, to examine the thermal properties of oils in their base state and in combination with additives, and also to better compare the results with other studies, a dimensioned system with a depth of 38 mm was constructed. Four sensors are placed inside the chamber at heights of 8 mm, 16 mm, 24 mm, and 32 mm from the chamber floor to measure the temperature of the PCM. The temperatures are recorded by a data acquisition system (Lurton TM-947SD model) with an accuracy of ±0.1 °C. To convert the heat stored by the PCMs into electricity, a thermoelectric module (SP1848-271 model) with dimensions of 40 mm × 40 mm is used at between the source of the PCM and the heat sink, generating electricity due to the temperature difference between its surfaces. The generated voltage is measured using a multimeter (DEC330FC model) with a precision of 1 mV. To achieve a greater temperature difference and electricity generation, an aluminium heat sink with dimensions of 35 mm × 35 mm x 30 mm is employed. Additionally, to maintain the heat sink at a low temperature (room temperature), a 50 ml water source is placed inside it over the experiment duration.

To prevent heat loss from the PCM chamber to the surrounding environment, the chamber was insulated with polyurethane foam during the experiment. This insulation aimed to increase the efficiency of heat transfer and thermal energy storage within the depth of the chamber. To adjust the light intensity, firstly, a shutter is placed above the chamber, and then the appropriate distance for an intensity of 900 W/m^2 is set in each test using the PCMs with a CMP3 secondary standard pyranometer, manufactured by Kipp & Zonen Co., with an accuracy of 1 W/m^2 in the wavelength range of 200–2800 nm. The total mass of the PCMs used in the study is 48 gr to fill the chamber, ensuring that the highest sensor is fully immersed in the PCM.

In each experiment, the PCM chamber as initially exposed to solar simulator irradiation at an intensity of 900 W/m^2 for 100 min. Following the termination of irradiation, the temperature variations of the PCM were monitored and recorded for an additional 100 min. It should be noted that in all the experiments, the initial temperature was the same to

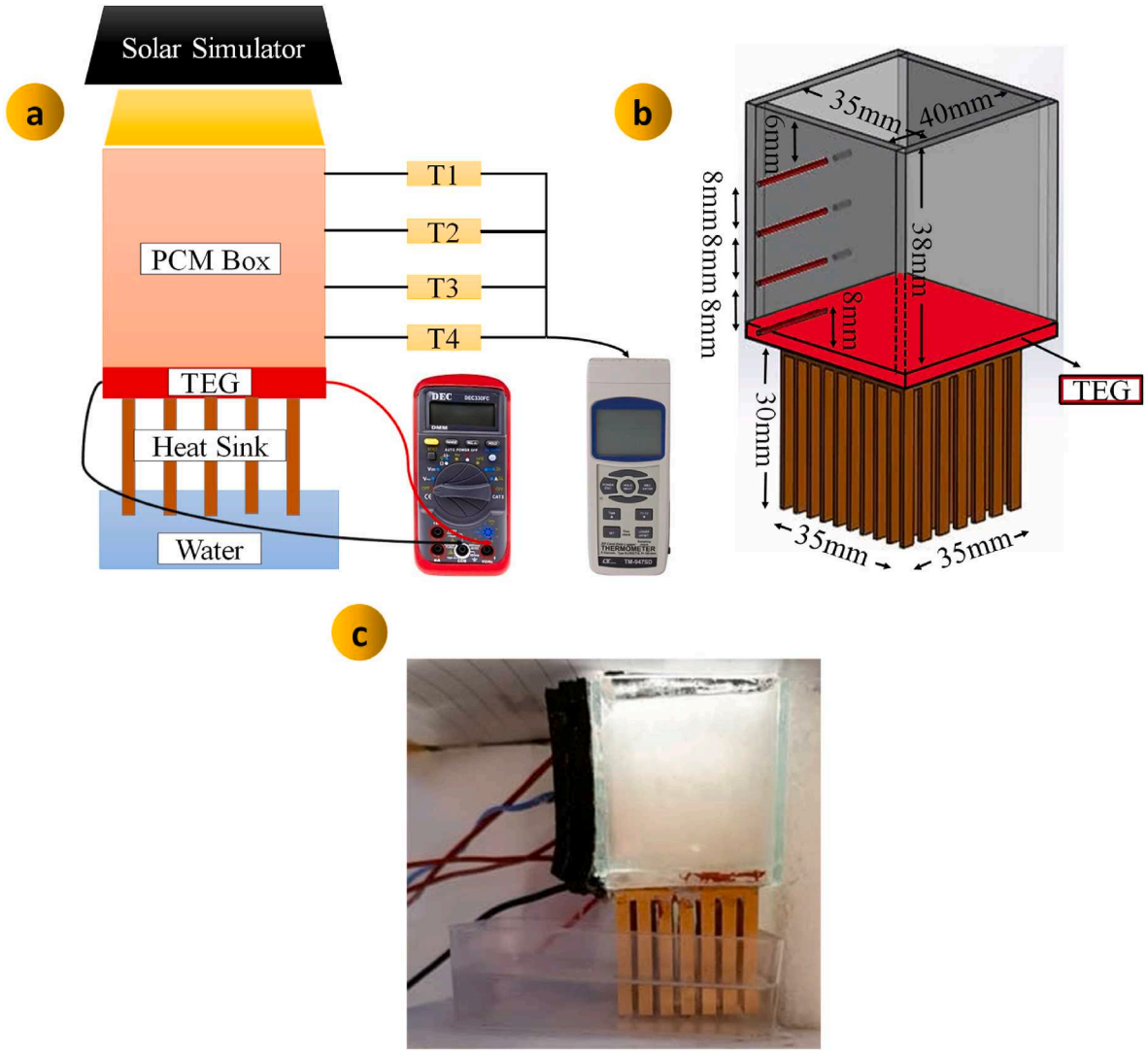

Fig. 1. (a) Two-dimensional schematic of the laboratory setup along with the utilized equipment. (b) Three-dimensional schematic of the studied system along with its precise dimensions. (c) Real image of the system.

ensure the same (22 °C) influence on their phase change behaviour.

3. Materials

The PCMs used in this study include Ostrich oil, mutton tallow, beef tallow, and coconut oil with melting temperature ranges of 23–24 °C, 20–23 °C, 22–23 °C, and 24–26 °C, respectively (Table 2). These materials were purchased from local stores. The thermal-physical properties of all oils are presented in Table 2. Furthermore, iron oxide nanoparticles with a diameter of 20 nm from VCN company were utilized to enhance heat transfer in the oils. Additionally, pine sawdust with dimensions of 100 μm were purchased from a local workshop. The scanning electron microscopy (SEM) images of pine sawdust and nanoparticles were taken using the VP 1450 model by LEO company and thermal properties of the nanoparticles and pine sawdust used in this study are presented in Fig. 2 and Table 3, respectively. While the thermal properties of iron oxide nanoparticles have been provided on Dekedao Gold Technology Company data sheets, the KD2 Pro device was employed to calculate the thermal conductivity of the carbonized sawdust. By placing a sensor inside a cube made of the sawdust of interest, thermal conductivity was determined by calculating the heat flux between the inside and outside of the cube.

To evaluate the thermophysical properties of PCMs, such as DSC (Differential Scanning Calorimetry) curves and thermal conductivity, the DS300 and KD2 Pro devices were employed sequentially. To validate the results of the PCMs, the properties recorded for coconut oil were compared with other articles which are presented in Table 4. As observed, the melting point of coconut oil has been reported in various studies to range from 22 to 28 °C [39–41], while the coconut oil utilized in this research exhibits a melting point of 24–26 °C. The reported values for latent heat of fusion in different articles vary within the range of 81–110 J/g due to variations in the source of coconut and the extracted fat content [42,43]. On the other hand, the latent heat of fusion in the present study has been determined to be 100 ± 7.5, which falls within

Table 2
Thermophysical properties of PCMs.

PCM	Beef tallow	Coconut oil	Mutton tallow	Ostrich oil
Specific heat capacity (kJ/kg.K)	2	1.89	1.9	1.6–2
Thermal conductivity (W/m.K)	0.16	0.166	0.23	0.17
Latent heat (kJ/kg)	10 ± 5	100 ± 7.5	7 ± 2	6 ± 3
Melting temperature (°C)	22–23	24–26	20–23	23–24
Density (kg/m^3)	760	800	770	780

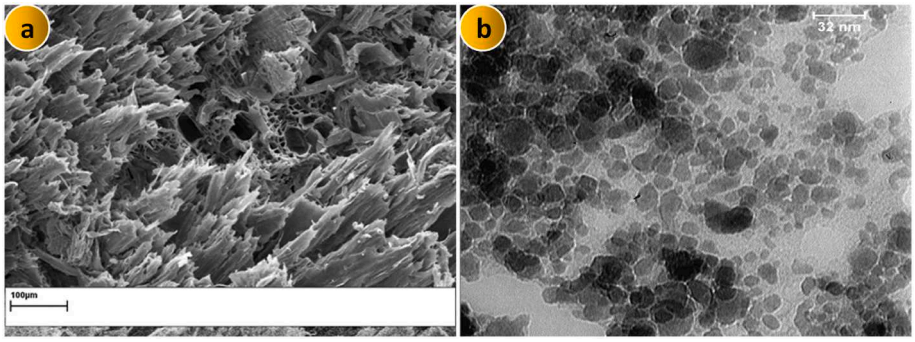

Fig. 2. SEM images of (a) pine sawdust and (b) Fe_3O_4 nanoparticles.

Table 3
Thermophysical properties of nanoparticles and sawdust.

Materials	Density (kg/m3)	Thermal conductivity (W/m.K)	Specific heat capacity (kJ/kg.K)	Particle size
Fe_3O_4 [37]	5180	80	670	10–20 nm
sawdust [38]	524	0.4	0.13	100 μm

Table 4
Comparison of the thermophysical properties of coconut oil studied in previous research with the findings of the present study.

Thermo-physical properties	Reported in literature	Present study
Melting point, (°C)	24 [40], 24.11 [39], 26.78 [41], 24–28 [42]	24–26
Latent heat, (J/g)	81.41 [39], 82 [43], 100 [42], 103 [40], 110.4 [41]	100 ± 7.5
Specific heat capacity (C_{pl}), (J/gk)	0.89 [39], 2 [40], 2.35 [43]	1.89 at 30 °C
Specific heat capacity (C_{ps}), (J/gk)	1.33 [39], 3.7 [40], 3.23 [43]	2.5 at 10 °C
Thermal conductivity, (W/mk)	0.165 [39], 0.166 [40], 0.32 [41]	0.166
Density, (kg/m^3)	914 [40], 924 [39]	800

the range of 81–110J/g. Additionally, the other thermophysical properties of PCMs such as specific heat capacity and thermal conductivity [39,40,43] also fall within the range of reported results in other articles (Table 4). In summary, the coconut oil examined in this study exhibits qualities that align closely with findings in existing literature, underscoring its consistency and trustworthiness across various experimental settings.

Due to the inability of coarse and high-density wood to remain stable inside the oil, low-density pine sawdust have been used. On the other hand, the sawdust surface alone does not have high sunlight absorption capability, hence carbonization of the sawdust surface has been carried out to enhance sunlight absorption [38]. For this purpose, pine sawdust are placed on a galvanized iron plate at a temperature of 200 °C for 60 s to undergo complete carbonization, as illustrated in Fig. 3 (in this study, carbonization was performed in air, but it is suggested that for greater expansion of the sawdust, this process be carried out in a nitrogen gas).

4. Preparation of PCM using carbonized sawdust and nanoparticles

In this study, iron oxide nanoparticles and carbonized sawdust were separately prepared in weight fractions of 0.3, 0.6, and 0.9 % (representing low, medium, and high concentrations) in the best PCM (coconut oil) in terms of energy storage. For that purpose, a quantity of 48 gr of the PCM was initially measured using an electronic scale (model PFB 2000–2, manufactured by Kern, with an accuracy of 0.1 gr). Next, the nanoparticles and carbonized sawdust were weighed using a more precise electronic scale (model BP121S, manufactured by Sartorius with an accuracy of 0.0001 gr). Subsequently, the best PCM was heated up. Following the complete melting, it was combined with different masses of nanoparticles and carbonized sawdust. An ultrasonic bath was used to enhance the stability, and interaction with the PCM, prevent settling, and avoid agglomeration of the nanoparticles. The samples were exposed to ultrasonic waves for 45 min at a power of 200 W and a frequency of 40 kHz. To maintain the molten state of the samples during ultrasonic treatment, they were placed in a water bath at 40 °C. Afterward, the samples (48 gr) were quickly removed from the ultrasonic bath and poured into the test chamber of the experimental system, where they were left to solidify and reach the ambient temperature

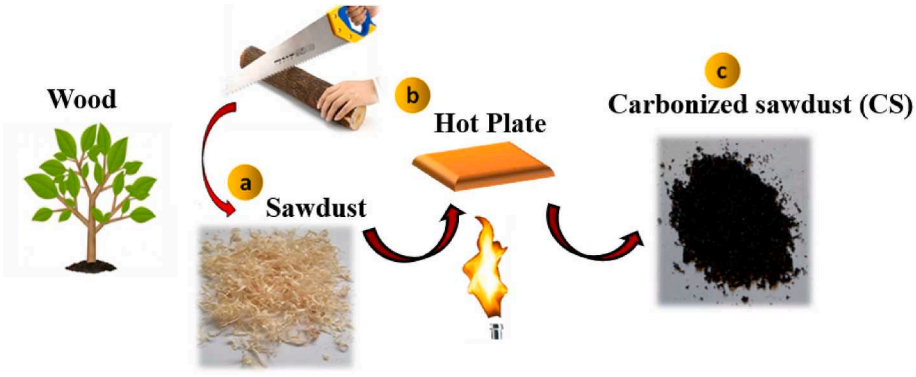

Fig. 3. Schematic of the carbonized sawdust (CS) preparation process: (a) Sawdust, (b) Carbonization at a surface temperature of 200 °C using a burner, (c) the CS.

(22 °C) in the laboratory to be ready for testing.

5. Results and discussions

In the following sections, the experimental results for four PCMs, namely ostrich oil, mutton tallow, beef tallow, and coconut oil, will be presented. The results will be analysed and discussed in terms of temperature variations, voltage measurements, energy storage capacity, and energy storage efficiency. Furthermore, the individual effects of iron oxide nanoparticles and carbonized sawdust on the photothermal conversion efficiency will be given for the best PCM.

5.1. The impact of photothermal conversion on PCMs

Fig. 4a displays the variations of specific heat capacity as a function of temperature for all the oils Differential Scanning Calorimetry (DSC) analysis has been employed to determine these properties. The coconut oil exhibits the highest enthalpy in the phase change region, as presented in Table 2. This is further supported by the larger area under its graph in Fig. 4a, indicating considerable changes in enthalpy at the initial temperature range of the test. However, the other oils, with their lower specific heat capacity and lower enthalpy compared to coconut oil, do not show a noticeable phase change range in comparison. Fig. 4b shows the temperature variations of the mentioned PCMs when the artificial solar radiation is on and off. Under artificial solar radiation conditions (for 100 min), the PCMs absorb the incident energy and transfer it from the surface to the interior of the PCM chamber through thermal conduction mechanisms. As it can be observed, the temperature during the irradiation process rises. As time progresses, the slope of the temperature curve gradually decreases, eventually reaching a relatively stable state. Ostrich oil, mutton tallow, and beef tallow, which have lower specific heat capacities exhibit a higher temperature increase slope during the radiation period compared to coconut oil. In the end of the period, the temperature reaches its peak, with ostrich oil recording the highest temperature of 35.5 °C, while coconut oil exhibits the lowest temperature at 34.5 °C. On the other hand, when the light radiation is turned off, the samples experience a rapid decrease in temperature, leading to a steep downward slope for all PCMs in the initial moments of radiation shutdown. However, over time and with the dissipation of heat to the surroundings, the gradient decreases. In comparison to other PCMs, coconut oil exhibits a slightly lower rate of temperature decrease. This is because it has a higher specific heat capacity compared to other materials.

Fig. 4c illustrates the voltage variations of the PCMs over the experiment time. The voltage changes correspond to the temperature variations as the electricity generated by the TEG depends on the temperature difference between the two sides. The maximum voltage generated among the PCMs is 75 mV for ostrich oil, while the minimum generated voltage is 68 mV for coconut oil. It is also observed that coconut oil shows a smaller gradient in voltage loss during temperature reduction in the absence of radiation. Therefore, even in the absence of radiation, PCMs continue to generate voltage. This generated voltage, during the absence of solar energy, is useful for compensating for the instability of the light source and consequently reducing electrical fluctuations. One can use the stored energy to generate voltage for several hours in order to reduce the limitation of access to solar energy. To evaluate the performance of a TEG, the electrical efficiency is a commonly used metric which can be obtained using the following formula [44].

$$\eta_{TEG} = \frac{\Delta T}{T_h} \frac{\sqrt{1+Z\overline{T}}-1}{\sqrt{1+Z\overline{T}}+\frac{T_c}{T_h}} \quad (1)$$

Where T_h and T_c represent the temperatures of the hot and cold sides of the TEG, respectively, and $\Delta T = T_h - T_c$ is the temperature difference across the thermoelectric material. $Z\overline{T}$ refers to the figure of merit (ZT) of the thermoelectric material, and η_{TEG} represents the electrical efficiency of the TEG module. In general, the commercially utilized thermoelectric materials in this study are based on telluride alloys, which have a $Z\overline{T}$ range of approximately 0.8 at room temperature [44]. In the $Z\overline{T}$ coefficient graphs for the material Bi_2Te_3, within the temperature range of the conducted research tests, this value is assumed to be relatively constant [45]. Therefore, the thermoelectric efficiency is dependent on ΔT. To determine the exact temperatures of the hot and cold sides of the thermoelectric module, thermal imaging was conducted using a thermal camera (model DT-980, with a temperature range of 20–80 °C), and the results presented in Fig. 4d and e. It was observed that the temperature data obtained from the thermal camera for the hot side of the thermoelectric module is approximately 0.4 °C lower than the temperature data from sensor number 4.

Fig. 4f presents the electrical efficiency of the thermoelectric materials over the experiment time. Since the temperature of the hot and cold sides of the thermoelectric module changes over time, the electrical efficiency is plotted as a function of time. It can be seen that at the beginning of the experiment, due to the smaller temperature difference between the cold and hot sides, the electrical efficiency is negligible. However, as the radiation time progresses and the temperature of the hot side increases, the temperature difference also increases, leading to the maximum electrical efficiency of the thermoelectric materials. The highest efficiency, reaching approximately 1.68 %, is achieved after 100 min of radiation for the ostrich oil. Furthermore, it is evident that coconut oil demonstrates inferior efficiency compared to other PCMs over the course of the 100-min radiation period. This can be attributed to the smaller temperature difference between the two sides of the thermoelectric module. After terminating the radiation, the stored heat is dissipated to the environment by the PCMs, causing a decrease in the temperature of the hot side of the thermoelectric module and a reduction in the temperature difference between the two sides. This results in a rapid decrease in the thermoelectric efficiency. During the absence of radiation, the higher energy storage by coconut oil and its slower temperature reduction rate led to a larger temperature difference between the two sides of the thermoelectric module. Therefore, in this situation, coconut oil shows higher electrical efficiency compared to other PCMs, and at the end of the experiment, due to the negligible temperature difference, the efficiency approaches zero.

To further investigate the conversion of sunlight to heat in PCMs, the energy storage capacity and the energy storage efficiency were calculated based on temperature changes and the specific heat capacity of the PCMs, as follows [21]:

$$Q_s = m \times \int c_p(T)dT \quad (2)$$

$$\eta = \frac{Q_s}{A \times I \times t} \quad (3)$$

Where Q_s (J/g) represents the amount of heat energy stored by the PCMs from the sunlight, and η denotes the energy storage efficiency at time t (s). m (g) is the mass of the PCMs, I (W/m^2) is the solar radiation power, and A (m^2) is the receiving area of direct sunlight. Additionally, the variations in the specific heat capacity of each PCM were obtained from the DSC results.

Fig. 5a and b illustrate the amount of stored heat and the energy storage efficiency of the PCMs during the radiation period (for 100 min), respectively. As shown in Fig. 5a, due to the higher specific heat capacity of coconut oil compared to other PCMs, it exhibits the highest energy storage capacity during the radiation period. It stores 33.9 J/g of energy after 100 min of radiation. On the other hand, mutton tallow, with its lower specific heat capacity compared to other PCMs, has the lowest energy storage capacity, storing only 18 J/g of energy.

In Fig. 5b, the variations in the energy storage efficiency of PCMs during the radiation period are presented. As observed, the energy storage efficiency of each PCM corresponds to their specific heat

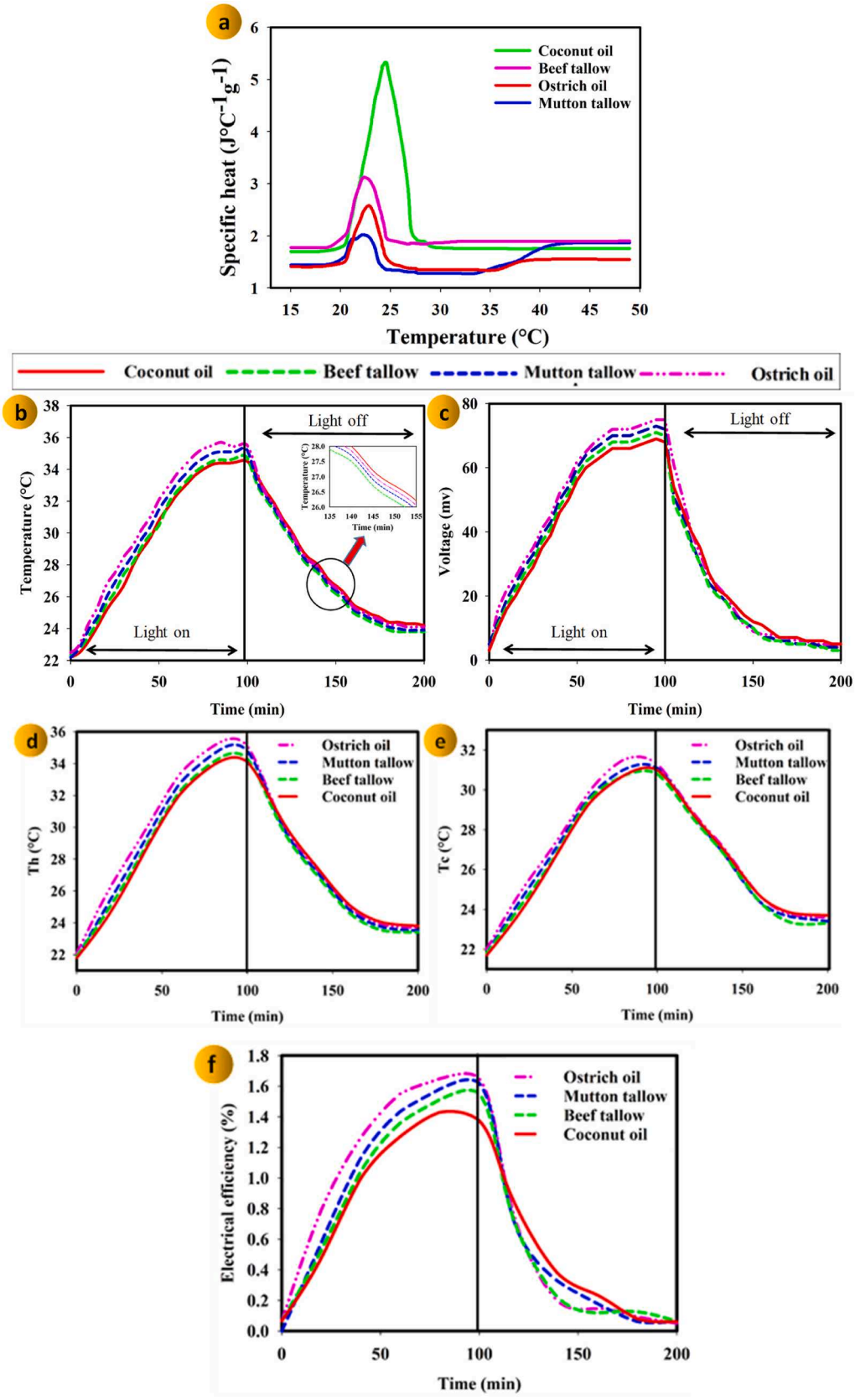

Fig. 4. (a) Results of the DSC test for coconut oil, mutton tallow, beef tallow, and ostrich oil, (b) Temperature variations of sensor number 4. (c) Voltage variations of the PCMs, (d) Temperature changes of the hot side of the TEG, (e) Temperature changes of the cold side of the TEG, (f) Thermoelectric efficiency variations of the PCMs.

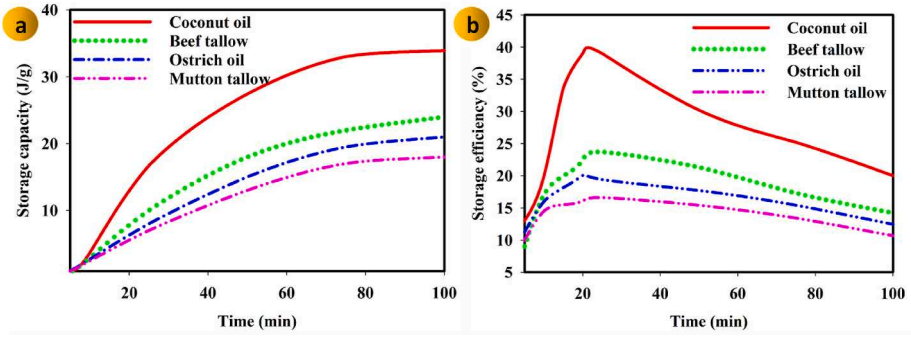

Fig. 5. (a) Energy storage capacity and (b) energy storage efficiency of the phase-change materials.

capacity variations (Fig. 4a). Among all the PCMs used in this study, coconut oil has a higher energy storage efficiency due to its higher specific heat capacity compared to other materials. Due to the rapid temperature increase trend at the beginning of the experiment, the maximum energy storage efficiency of the PCMs occurred in the initial part of the experiment. As observed, coconut oil demonstrates the highest energy storage efficiency at 39 %, whereas mutton tallow exhibits the lowest efficiency at 16.59 %. Following the initial increase, there is a declining trend in the energy storage efficiency of all PCMs over time. The decrease occurs due to the constancy of enthalpy and the reduction in the slope of temperature increase. As depicted in Fig. 4a, the specific heat capacity of PCMs decreases and eventually stabilizes after a certain period, as shown in Fig. 5a. This change in specific heat capacity, alongside the reduction in the slope of temperature increase during the test, has caused the slope of the energy storage curve to decrease over time.

5.2. Exergy of PCMs

The exergy of PCMs in solid, liquid, and two-phase (solid-liquid) states during the experiment can be determined using Eq. (4) [46]:

$$\Psi_{PCM} = mC_{ps}\left[T_s - T_{ini} - T_0 \ln\frac{T_s}{T_{ini}}\right] + mC_{pa}\left[T_l - T_s - T_0 \ln\frac{T_l}{T_s}\right] + mC_{pl}\left[T_{fin} - T_l - T_0 \ln\frac{T_{fin}}{T_l}\right] \quad (4)$$

In equation (4), T_{ini} represents the initial temperature of the experiment, T_s is the starting temperature of the phase change from solid to liquid, T_l is the temperature of the liquid after the end of the phase change, and T_{fin} is the final temperature of the test. For three states: solid, two-phase, and liquid, the specific heat capacities are denoted respectively by C_{ps}, C_{pa}, and C_{pl}. Furthermore, the exergy absorbed from solar radiation at the surface of the PCM source can be calculated according to Eq. (5) [46]:

$$\Psi_{sun} = \int_0^t AI\left[1 + \frac{1}{3}\left(\frac{T_{amb}}{T_{sun}}\right)^4 - \frac{4}{3}\left(\frac{T_{amb}}{T_{sun}}\right)\right]dt \quad (5)$$

Where A (m^2) is the cross-sectional area exposed to the radiation of the PCM, and T_{sun} is the temperature of the sun (6000 K). The exergy efficiency of a PCM can be obtained by dividing the exergy gained from the PCM, Ψ_{PCM}, by the exergy input from solar radiation, Ψ_{sun}, as follows [46]:

$$\eta_{ex} = \frac{\Psi_{PCM}}{\Psi_{sun}} \quad (6)$$

In Fig. 6a and b, the exergy and exergy storage efficiency of Phase Change Materials (PCMs) during the radiation period (lasting 100 min) are depicted, respectively. As anticipated, the exergy storage curve of the PCMs (Fig. 6a) mirrors the energy storage curve (Fig. 5a). For instance, at the beginning of the experiment, coconut oil exhibits a steeper exergy curve due to its maximum specific heat capacity in the phase change region (Fig. 4a). Conversely, towards the end of the experiment, following complete melting, the specific heat capacity stabilizes, causing the exergy variation curve for coconut oil to approach zero. Consequently, coconut oil achieves the highest stored exergy, reaching 426.28 J, whereas beef tallow shows the lowest stored exergy at 239.02 J. Fig. 6b presents the exergy storage efficiency of PCMs, including the uncertainty derived from three repetitions of the experiment. It is evident that the exergy storage efficiency curves correspond to the exergy variation curves (Fig. 6a). For different PCMs, the exergy storage efficiency initially increases due to the steep slope of temperature changes and the high specific heat capacity, as indicated by Eq. (6). However, over time, as the slope of exergy variations decreases, the exergy storage efficiency declines, reaching its lowest point by the end of the experiment. This trend is attributable to the constant rate of exergy absorption from solar radiation, as calculated using Eq. (5). In other words, the stored exergy, based on Eq. (4), is influenced by temperature changes and the heat capacity of the PCMs during the phase change process. This stored exergy includes contributions from the solid, two-

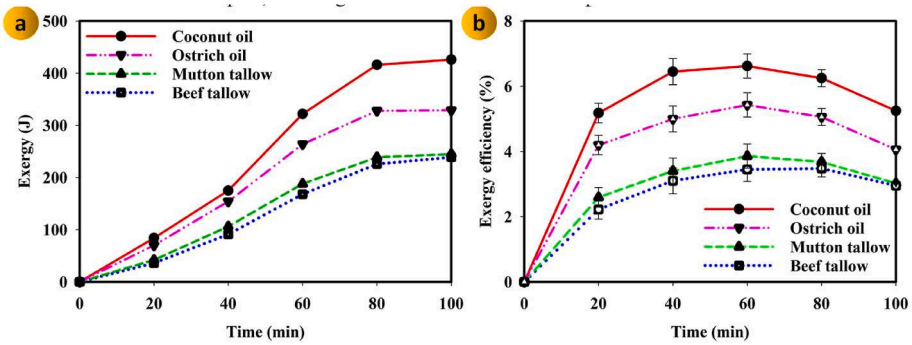

Fig. 6. (a) Variations of stored exergy and (b) exergy storage efficiency of PCMs.

phase, and liquid states. Therefore, determining the specific heat capacity (Cp) at each temperature requires the start and end temperatures of the test, as well as the melting start and end temperatures from the specific heat capacity curve, as shown in Fig. 4(a) and 8. Based on these factors, coconut oil demonstrates higher energy storage efficiency due to its superior heat capacity, optimal melting point for absorbing and storing solar energy, high capacity for solar radiation absorption, and uniform heat distribution during the phase change process. Therefore, the highest and lowest energy storage efficiencies during the 100-min test period are observed for coconut oil and tallow oil, with values of 6.3 % and 3.3 %, respectively.

In summary, exergy efficiency directly reflects the proportion of input solar energy that is stored as useful work. PCMs with higher exergy efficiency typically ensure more uniform heat distribution, which prevents the formation of hot and cold spots, resulting in more stable and efficient performance over time.

5.3. Combining the superior PCM with iron oxide nanoparticles and carbonized sawdust

Given the superior performance of coconut oil in converting sunlight to heat and its high energy storage capacity compared to other PCMs, we conducted individual studies to investigate the effects of combining it with iron oxide nanoparticles and carbonized sawdust particles separately. These studies focused on examining the impact of these combinations on temperature changes, voltage changes, energy storage, and PCM energy storage efficiency. Fig. 7a and b presents the results of absorption spectrum tests conducted on each combination (nanoparticles or CS) with PCM for each weight percentage, under conditions where the sample is in a liquid state, using a spectrophotometer (Agilent 8453 Model). The findings indicate that coconut oil alone has limited capability to absorb sunlight, whereas after combining with each additive, the absorption of sunlight in the base liquid significantly increases. In Fig. 7a, it is evident that carbonized sawdust at a concentration of 0.9 % can increase the light absorption capacity of the PCM by up to 7 times. Furthermore, Fig. 7b shows that the combination of coconut oil and iron oxide nanoparticles has a more pronounced effect on the absorption of visible sunlight. With the increase of nanoparticle concentration to 0.9 %, the sunlight absorption in coconut oil is 8.9 times greater than pure coconut oil. As a result, these two materials have been selected as promising candidates for further evaluation.

Furthermore, the analysis of parameters that affect heat losses is crucial in this study. Among these parameters, thermal conductivity plays a significant role in determining the heat losses in the composite of nanoparticles and CS with coconut oil. The thermal conductivity can be determined using the Maxwell equation [47] (Eq. (7)), and the corresponding results are presented in Fig. 7c.

$$k_{eff} = \frac{2k_{Co} + k_{Nano} + 2\varnothing(k_{Nano} - k_{Co})}{2k_{Co} + k_{Nano} - \varnothing(k_{Nano} - k_{Co})} .k_{Co} \quad (7)$$

Where k_{Co} , k_{Nano} represent the thermal conductivity of coconut oil, and iron oxide nanoparticles and carbonized sawdust, respectively, and $\varnothing$ denotes the volume fraction of nanoparticles and carbonized sawdust in coconut oil. As depicted in Fig. 7c, since the nanoparticles are metal-based and possess high thermal conductivity, their combination with coconut oil results in a higher thermal conductivity compared to the combinations containing CS particles. The thermal conductivity of the base fluid increases by adding 0.9 % iron oxide nanoparticles by 3.5 % (from 0.166 to 0.172 W/m·K), while the maximum increase for carbonized wood particles is observed to be 1.2 % (from 0.166 to 0.168

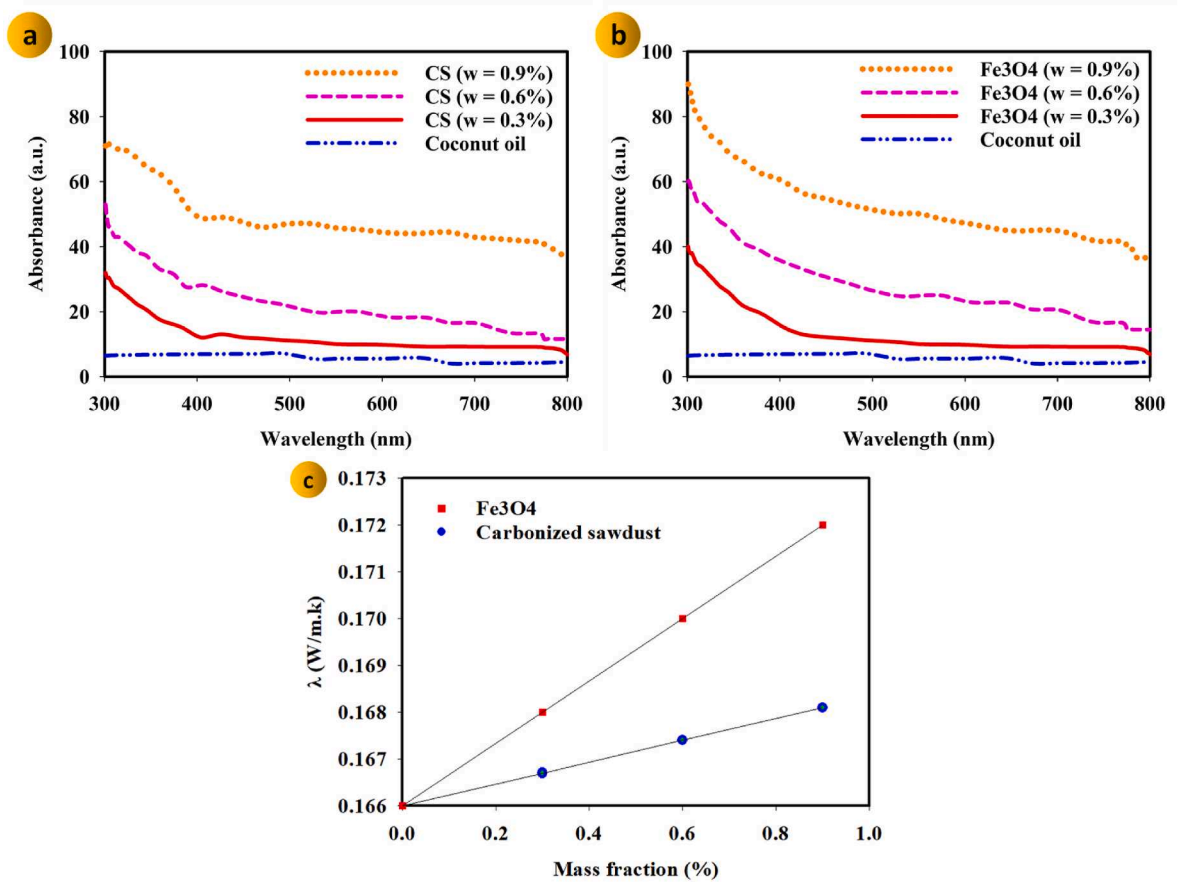

Fig. 7. The results of the sunlight absorption test for coconut oil with: (a) carbonized sawdust (CS) and (b) iron oxide nanoparticles at mass percentages of 0.3 %, 0.6 %, and 0.9 % compared to pure coconut oil, (c) The thermal conductivity coefficient of coconut oil for different mass fraction of iron oxide nanoparticles and CS.

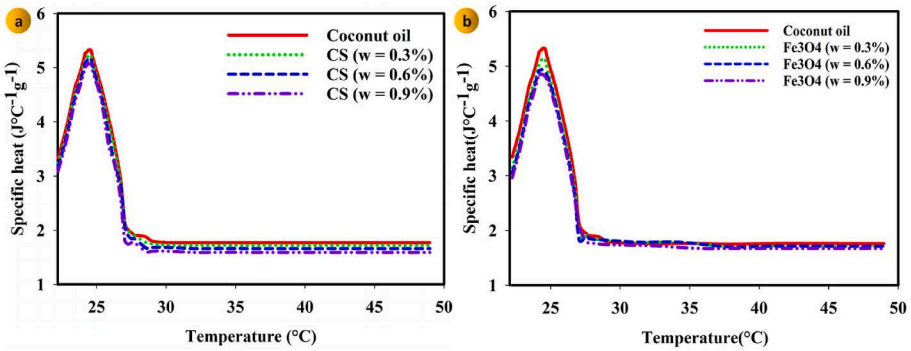

Fig. 8. The specific heat capacity of coconut oil with (a) carbonized sawdust and (b) iron oxide nanoparticles.

W/m·K).

Fig. 8a and b illustrate the variations in specific heat capacity of carbonized sawdust and iron oxide nanoparticles in coconut oil, respectively. It can be observed that the addition of nanoparticles does not significantly change the specific heat capacity (Cp) of the solution, primarily due to the small amount of additives. This results in only a negligible change in the storage capacity of the chamber. Therefore, the notable impact of these additives, along with increased heat absorption, is the significant improvement in thermal conductivity and more uniform heat distribution within the chamber.

Fig. 9(a–d) illustrates the experimental results of temperature and voltage variations in pure coconut oil and its combinations with iron oxide nanoparticles and carbonized sawdust at mass fraction of 0.3 %, 0.6 %, and 0.9 %. Since the PCMs have transformed into a liquid state after absorbing radiation, the maximum temperature at the end of the experiment primarily depends on the sunlight absorption capability of the PCM in its liquid state. As observed, compared to pure coconut oil, the temperature of coconut oil enhanced with nanoparticles increases more rapidly during the simulated sunlight radiation and reaches higher maximum temperatures. Furthermore, all samples reach a stable state under solar radiation. For example, the sample with the lowest mass fraction (0.3 %) of iron oxide nanoparticles (Fig. 9a) and carbonized sawdust (Fig. 9c) achieve temperatures of 35.8 °C and 34.9 °C, respectively, after 100 min. With an increase in the concentration of nanoparticles and carbonized sawdust to 0.9 %, the temperatures rise to 38.5 °C and 36.3 °C, respectively. The iron oxide nanoparticles, due to their black colour, result in an increased sunlight absorption capability, as shown in Fig. 7b. Moreover, these nanoparticles possess a high

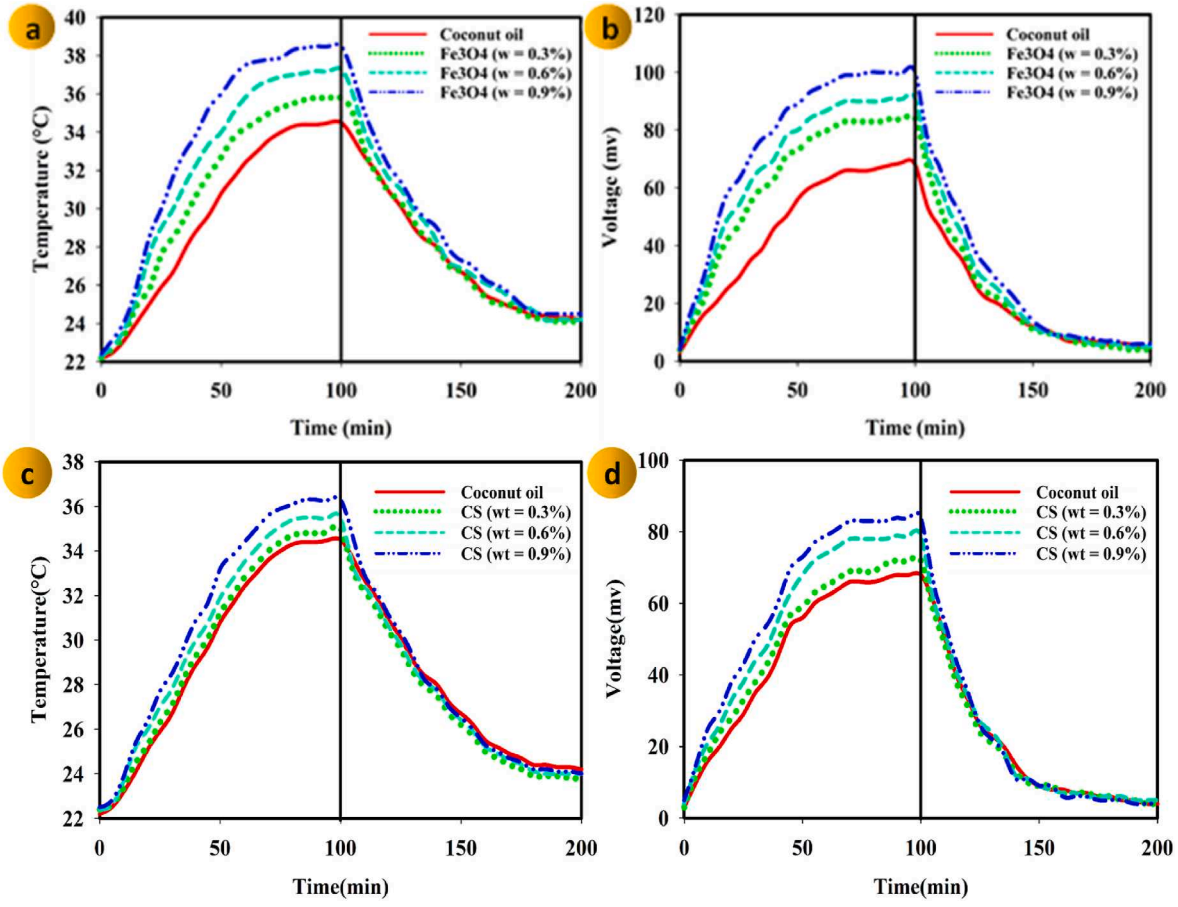

Fig. 9. (a) Temperature variations of sensor number 4 in the presence of nanoparticles. (b) Voltage changes with the presence of nanoparticles. (c) Temperature variations of sensor number 4 accompanied by carbonized sawdust (CS). (d) Voltage changes accompanied by CS particles.

thermal conductivity coefficient, which leads to an overall enhancement in the thermal conductivity when combined with pure coconut oil, as depicted in Fig. 7c. This enhanced thermal conductivity contributes to an increased heat transfer from the upper part of the PCM chamber to the lower part, allowing for efficient heat transfer. On the other hand, due to the complete carbonization of the sawdust, when exposed to ultrasonic wave irradiation, a portion of the carbon on their surface is dispersed into the coconut oil, resulting in increased sunlight absorption in the coconut oil, shown in Fig. 7a. However, the temperature variations in the combination containing carbonized sawdust exhibit only a slight difference compared to pure coconut oil at the lowest mass percentage (0.3 %). However, as the mass fraction of carbonized sawdust increases, the temperature variations increase due to the enhanced sunlight absorption by the carbonized sawdust. Furthermore, during the cooling process, it is observed that combinations containing nanoparticles exhibit steeper temperature decline compared to combinations containing carbonized sawdust, due to better heat transfer to the surroundings.

Moreover, the voltage variations are also shown in Fig. 9b and d. During the period of sunlight (for 100 min), as the concentration of nanoparticles in coconut oil increases, the voltage curves exhibit a steeper slope (Fig. 9b) compared to the combinations containing carbonized sawdust (Fig. 9d), leading to a more rapid increase in voltage. This behaviour can be attributed to the enhanced heat transfer facilitated by iron oxide nanoparticles and the larger temperature difference between the two sides of the thermoelectric module. For example, at the minimum mass fraction of iron oxide nanoparticles and carbonized sawdust (0.3 %), they generated voltages of 84 and 72 mV, respectively, within a span of 100 min. At the maximum mass fraction (0.9 %), they produced voltages of 100 and 84 mV, respectively. Therefore, the maximum concentration of nanoparticles and CS resulted in an improvement of 47 % and 23.5 % in the generated voltage, respectively, when compared to pure coconut oil. Furthermore, voltage production persists during the cooling phase, and combinations containing nanoparticles exhibit a more pronounced decline in voltage compared to combinations containing carbonized sawdust. However, as the testing period nears its end, this difference becomes insignificant.

The energy storage capacity and thermal efficiency of the coconut oil mixture with iron oxide nanoparticles and carbonized sawdust are presented in Fig. 10. It can be observed that the addition of iron oxide nanoparticles to coconut oil leads to a further increase in energy storage during the irradiation period. According to Fig. 10a, in the initial minutes of the test, combinations containing nanoparticles exhibit higher energy storage compared to pure coconut oil. This is due to the enhanced heat transfer and temperature increase compared to pure coconut oil. Hence, the highest concentration of iron oxide nanoparticles (0.9 %) achieved the highest solar energy storage capacity of 39 J/g, among all samples during the 100-min duration. This value was reported as 33.9 J/g for pure coconut oil, representing the highest temperature obtained after 100-min of irradiation. Furthermore, due to the steep increase in temperature at the beginning of the experiment, the maximum thermal efficiency occurred during the initial minutes. This is because there was relatively low heat loss during the early stages, and the highest amount of absorbed heat was utilized for the phase change of the material. Additionally, when the PCM transitioned into a liquid state (i.e., volumetric absorber), heat loss increased significantly due to the higher temperature, resulting in a decrease in thermal efficiency with increasing heating time. Consequently, the sample with a higher mass concentration (0.9 %) obtained a greater thermal energy storage efficiency in the liquid state, approximately 62 %.

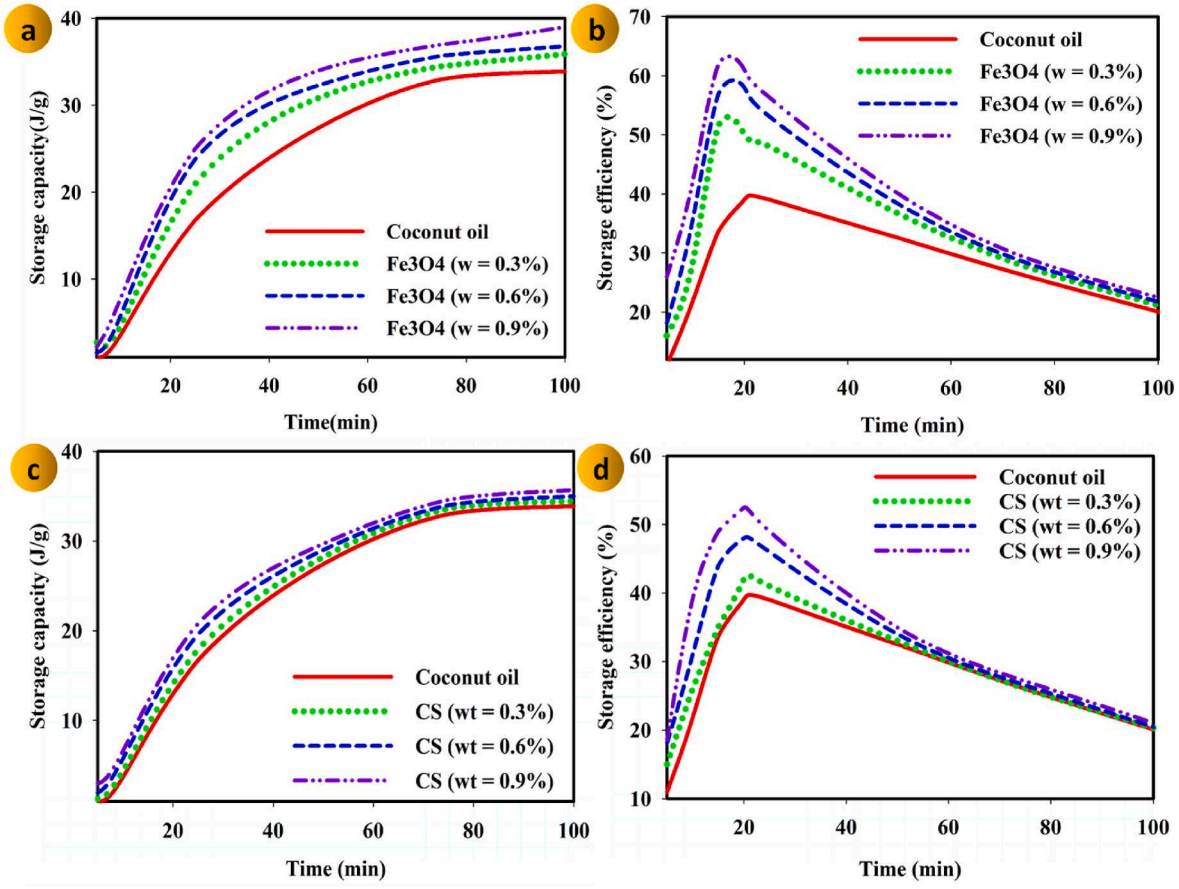

Fig. 10. (a) Variations in energy storage capacity by samples containing nanoparticles, (b) Thermal efficiency of samples containing nanoparticles, (c) Variations in energy storage capacity by samples containing carbonized sawdust (CS), (d) Thermal efficiency of samples containing CS particles.

Fig. 10c and d presents the energy storage capacity and thermal energy storage efficiency, respectively, for various compositions of carbonized sawdust. As observed, during the initial minutes of the experiment, where heat transfer did not differ significantly compared to pure coconut oil, the energy storage capacity of samples containing carbonized sawdust showed only slight differences. However, after increasing the heat transfer, the sample with the highest concentration of carbonized sawdust (0.9 %) demonstrated the highest solar energy storage capacity (35 J/g) among all the samples, similar to the samples containing nanoparticles. This corresponds to the highest temperature achieved after 100 min of irradiation. Moreover, as shown in Fig. 10d, due to a more pronounced temperature increase in compositions containing carbonized sawdust compared to pure coconut oil, the highest efficiency was observed during the initial minutes of the experiment. Additionally, after receiving heat and transitioning to a liquid state, the samples experienced significant heat loss at high temperatures. Consequently, as the heating time increased, the efficiency decreased. Therefore, the sample with a higher mass concentration (0.9 %) achieved a greater heat efficiency of 53 %.

In Fig. 11, the exergy and exergy efficiency of the samples containing iron oxide nanoparticles and carbonized sawdust are presented compared to coconut oil. Fig. 11a and c shows the variations in stored exergy by samples containing nanoparticles and CS particles, respectively. As observed, the amount of stored exergy in coconut oil reinforced with nanoparticles (Fig. 11a) increases at a higher rate compared to compositions containing CS particles (Fig. 11c) over 100 min, due to a faster temperature increase. Consequently, samples containing nanoparticles achieve a higher maximum exergy after 100 min. In other words, the nanoparticles with the highest mass fraction (%9.0) of iron oxide and CS particles respectively store 584.21 J and 476.78 J, while pure coconut oil records a value of 426 J. This trend is also evident in Fig. 11b and d, illustrating the variations in exergy efficiency of samples containing nanoparticles and carbonized sawdust. After 60 min, due to the relative decrease in specific heat capacity in samples containing nanoparticles (Fig. 8b) and CS particles (Fig. 8a), along with the stability of temperature in samples containing nanoparticles (Fig. 9a) and CS particles (Fig. 9c), the exergy efficiency declines. Therefore, the energy storage efficiency achieved by the highest mass percentage (0.9 %) of iron oxide nanoparticles and CS particles during the 100-min experiment was recorded as 10 % and 7.9 %, respectively.

6. Conclusions

In this study, an experimental investigation was conducted to examine edible PCMs (ostrich oil, mutton tallow, beef tallow, and coconut oil) for solar energy storage and electricity generation. Moreover, the performance of these PCMs, in terms of energy storage capacity and efficiency, were evaluated along with the use of additive substances. To enhance heat conductivity and sunlight absorption, the impact of incorporating iron oxide nanoparticles and carbonized sawdust (CS) into coconut oil was examined. The findings indicate that without any additives, ostrich oil and coconut oil exhibited the highest and lowest temperature changes during solar radiation, respectively. For a more comprehensive comparison of the edible PCMs, the analysis focused on energy storage capacity, energy storage efficiency, specific heat capacity, and temperature variations. Coconut oil and mutton tallow showed the highest and lowest energy storage capacities, respectively, while coconut oil and beef tallow exhibited in turn the highest and lowest stored exergy. Based on the evaluation of the stored heat energy, energy storage efficiency, and voltage sustainability after solar energy interruption, coconut oil was selected as the superior PCM compared to the other edible PCMs. The presence of iron oxide nanoparticles in coconut

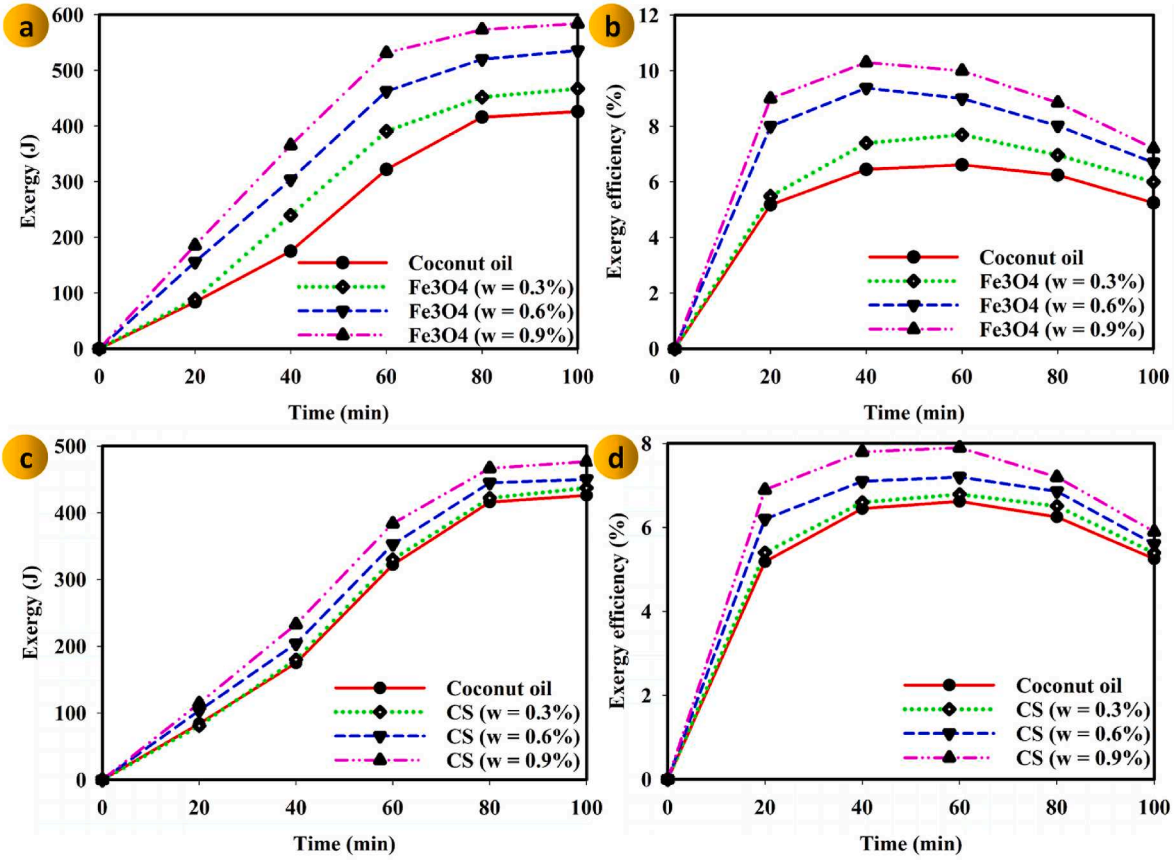

Fig. 11. Variations in (a) stored exergy and (b) exergy efficiency of samples containing nanoparticles, (c) stored exergy and (d) exergy efficiency of samples containing carbonized sawdust particles.

oil resulted in a 11.5 % increase in temperature and a 47 % increase in generated voltage over a 100-min period. Additionally, the energy storage capacity and energy storage efficiency increased by 15 % and 31.1 %, respectively, compared to pure coconut oil. Furthermore, the stored exergy and exergy efficiency increased by 37 % and 3.7 %, respectively, compared to pure coconut oil after 100 min carbonized sawdust had less effect on solar photothermal conversion of coconut oil due to their lower heat conductivity compared to iron oxide nanoparticles. However, their black surface led to an increase in solar radiation absorption, resulting in a 5.2 % increase in temperature and a 23.5 % increase in generated voltage over 100 min. Moreover, the stored energy and energy storage efficiency increased by 3.2 % and 19.1 %, respectively, compared to pure coconut oil. Additionally, the stored exergy and exergy efficiency increased by 11.87 % and 1.6 %, respectively, compared to pure coconut oil after 100 min. Nevertheless, due to the higher thermal conductivity of nanoparticles compared to CS particles, nanoparticles exhibited higher energy storage and electricity generation capabilities. In general, the results of this study prove that improving solar heat storage efficiency and electricity generation rate from that with a readily available, renewable, and low-cost material is surely a possibility. However, further investigation is required to explore other strategies and approaches to enhance the absorption and thermal conductivity coefficient of coconut oil with carbonized sawdust.

CRediT authorship contribution statement

Ali Mortazavi: Software, Resources, Methodology. **Emadoddin Erfani Farsi Eidgah:** Visualization, Methodology, Conceptualization. **Mohammad Mustafa Ghafurian:** Writing – review & editing, Writing – original draft, Project administration, Methodology, Formal analysis, Conceptualization. **Saleh S. Meibodi:** Writing – original draft. **Ali Kianifar:** Supervision. **Ahmad Arabkoohsar:** Writing – review & editing, Conceptualization.

Declaration of competing interest

The authors declare that they have no known competing financial interests or personal relationships that could have appeared to influence the work reported in this paper.

Data availability

No data was used for the research described in the article.

References

[1] Welsby D, Price J, Pye S, Ekins P. Unextractable fossil fuels in a 1.5 °C world. Nature 2021;597(7875):230–4.
[2] Rahman A, Farrok O, Haque MM. Environmental impact of renewable energy source based electrical power plants: solar, wind, hydroelectric, biomass, geothermal, tidal, ocean, and osmotic. Renew Sustain Energy Rev 2022;161:112279.
[3] Silva S, Laranjeira E, Soares I. Health benefits from renewable electricity sources: a review. Energies 2021;14(20):6678.
[4] Kannan N, Vakeesan D. Solar energy for future world: - a review. Renew Sustain Energy Rev 2016;62:1092–105.
[5] Hayat MB, Ali D, Monyake KC, Alagha L, Ahmed N. Solar energy—A look into power generation, challenges, and a solar-powered future. Int J Energy Res 2019;43:1049–67. https://doi.org/10.1016/10.1002/er.4252.
[6] Maka AOM, Alabid JM. Solar energy technology and its roles in sustainable development. Clean Energy 2022;6(3):476–83.
[7] Du X, Wang S, Du Z, Cheng X, Wang H. Preparation and characterization of flame-retardant nanoencapsulated phase change materials with poly (methylmethacrylate) shells for thermal energy storage. J Mater Chem A 2018;6(36):17519–29.
[8] Alva G, Lin Y, Fang G. An overview of thermal energy storage systems. Energy 2018;144:341–78.
[9] Sarbu I, Sebarchievici C. A comprehensive review of thermal energy storage. Sustainability 2018;10.
[10] Kapsalis V, Karamanis D. Solar thermal energy storage and heat pumps with phase change materials. Appl Therm Eng 2016;99:1212–24.
[11] Irani M, Ghafurian MM, Khorasani MM, Mehrkhah R, Mahian O. A comparative study of the effect of phase change material (paraffin wax) on volumetric and surface direct solar steam generation. J Taiwan Inst Chem Eng 2021;128:253–60.
[12] Sui X, Li W, Zhang Y, Wu Y. Theoretical and experimental evaluation of a thermoelectric generator using concentration and thermal energy storage. IEEE Access 2020;8:87820–8.
[13] Maleki Y, Pourfayaz F, Mehrpooya M. Experimental study of a novel hybrid photovoltaic/thermal and thermoelectric generators system with dual phase change materials. Renew Energy 2022;201:202–15.
[14] Khan MS, Abid M, Bashir MA, Amber KP, Khanmohammadi S, Yan M. Thermodynamic and exergoeconomic analysis of a novel solar-assisted multigenerational system utilizing high temperature phase change material and hybrid nanofluid. Energy Convers Manag 2021;236:113948.
[15] Gao W, Li J, Li Y, Kong L. Numerical identification of critical erosion prone areas in tube heat exchangers. Engineering Applications of Computational Fluid Mechanics 2020;14(1):1429–44.
[16] Mofijur M, et al. Phase change materials (PCM) for solar energy usages and storage: an overview. Energies 2019;12(16):3167.
[17] Luo X, Guo Q, Tao Z, Liang Y, Liu Z. Modified phase change materials used for thermal management of a novel solar thermoelectric generator. Energy Convers Manag 2020;208:112459.
[18] Nourani M, Hamdami N, Keramat J, Moheb A, Shahedi M. Thermal behavior of paraffin-nano-Al2O3 stabilized by sodium stearoyl lactylate as a stable phase change material with high thermal conductivity. Renew Energy 2016;88:474–82.
[19] Zhang H, Wang L, Xi S, Xie H, Yu W. 3D porous copper foam-based shape-stabilized composite phase change materials for high photothermal conversion, thermal conductivity and storage. Renew Energy 2021;175:307–17.
[20] Chen M, He Y, Ye Q, Zhang Z, Hu Y. Solar thermal conversion and thermal energy storage of CuO/Paraffin phase change composites. Int J Heat Mass Tran 2019;130:1133–40.
[21] Shi L, Hu Y, Bai Y, He Y. Dynamic tuning of magnetic phase change composites for solar-thermal conversion and energy storage. Appl Energy 2020;263:114570.
[22] Cao Z, Li W. A day-night solar thermoelectric generator enabled by phase change material and forced water cooling. Sol Energy 2024;268:112315.
[23] Reyes-Cueva E, Nicolalde JF, Martínez-Gómez J. Characterization of unripe and mature avocado seed oil in different proportions as phase change materials and simulation of their cooling storage. Molecules 2021;26(1):107.
[24] Fabiani C, Pisello AL, Barbanera M, Cabeza LF, Cotana F. Assessing the potentiality of animal fat based-bio phase change materials (PCM) for building applications: an innovative multipurpose thermal investigation. Energies 2019;12(6):1111.
[25] Thaib R, Amin M, Umar H. Thermal properties of beef tallow/coconut oil bio PCM using T-history method for wall building applications. European Journal of Engineering Research and Science 2019;4:38–40.
[26] Jurčević M, Nižetić S, Čoko D, Hoang AT, Papadopoulos AM. Experimental investigation of novel hybrid phase change materials. Clean Technol Environ Policy 2022;24(1):201–12.
[27] Kahwaji S, White MA. Edible oils as practical phase change materials for thermal energy storage. Appl Sci 2019;9(8):1627.
[28] Liu X, et al. Biomass-based phase change material gels demonstrating solar-thermal conversion and thermal energy storage for thermoelectric power generation and personal thermal management. Sol Energy 2022;239:307–18.
[29] Lin SC, Al-Kayiem HH. Thermal reliability of paraffin wax phase change material for thermal energy storage. Appl Mech Mater 2015;699:263–8.
[30] Ojike O, Okonkwo WI. Study of a passive solar air heater using palm oil and paraffin as storage media. Case Stud Therm Eng 2019;14:100454.
[31] Agyenim F. The use of enhanced heat transfer phase change materials (PCM) to improve the coefficient of performance (COP) of solar powered LiBr/H2O absorption cooling systems. Renew Energy 2016;87:229–39.
[32] Ahmed SF, et al. Integration of phase change materials in improving the performance of heating, cooling, and clean energy storage systems: an overview. J Clean Prod 2022;364:132639.
[33] Balakrishnan DBK, Sanandharya K, Anand S, Kumar S. Experimental study on solar cooker using phase change materials. Appl Mech Mater 2015;766–767:463–7.
[34] Saleel CA. A review on the use of coconut oil as an organic phase change material with its melting process, heat transfer, and energy storage characteristics. J Therm Anal Calorim 2022;147(7):4451–72.
[35] Safira L, Putra N, Trisnadewi T, Kusrini E, Mahlia TMI. Thermal properties of sonicated graphene in coconut oil as a phase change material for energy storage in building applications1. Int J Low Carbon Technol 2020;15(4):629–36.
[36] Soodoo N, Poopalam KD, Bouzidi L, Narine SS. Fundamental structure-function relationships in vegetable oil based phase change materials: a critical review. J Energy Storage 2022;51:104355.
[37] Wang J, Li Y, Zheng D, Mikulčić H, Vujanović M, Sundén B. Preparation and thermophysical property analysis of nanocomposite phase change materials for energy storage. Renew Sustain Energy Rev 2021;151:111541.
[38] Ghafurian MM, et al. Interfacial solar steam generation by sawdust coated with W doped VO2. Energy 2022;244:123146.
[39] Dhamodharan P, Bakthavatsalam AK. Experimental investigation on thermophysical properties of coconut oil and lauryl alcohol for energy recovery from cold condensate. J Energy Storage 2020;31:101639.
[40] Ebadi S, Humaira Tasnim S, Abbas Aliabadi A, Mahmud S. Geometry and nanoparticle loading effects on the bio-based nano-PCM filled cylindrical thermal energy storage system. Appl Therm Eng 2018;141:724–40.
[41] Wi S, Seo J, Jeong S-G, Chang SJ, Kang Y, Kim S. Thermal properties of shape-stabilized phase change materials using fatty acid ester and exfoliated graphite

nanoplatelets for saving energy in buildings. Sol Energy Mater Sol Cell 2015;143:168–73.
[42] Erfani Farsi Eidgah E, Ghafurian MM, Tavakoli A, Mortazavi A, Kianifar A. Solar-thermal conversion and thermal energy storage of different phase change materials. J Therm Anal Calorim 2023;148(16):8051–60.
[43] S. Wonorahardjo, I. M. Sutjahja, D. Kurnia, Z. Fahmi, and W. A. Putri, "Potential of thermal energy storage using coconut oil for air temperature control," Buildings, vol. 8, no. 8. doi: 10.3390/buildings8080095..
[44] Cao R, et al. Enhancing solar–thermal–electric energy conversion based on m-PEGMA/GO synergistic phase change aerogels. J Mater Chem A 2020;8(26):13207–17. https://doi.org/10.1039/D0TA04712K.
[45] Reyes-Gil KR, Whaley J, Nishimoto R, Yang N. Development of transport properties characterization capabilities for thermoelectric materials and modules, vol. 1774. MRS Online Proceedings Library (OPL); 2015. p. 7–12.
[46] Yang L, Zhang X, Xu G. Thermal performance of a solar storage packed bed using spherical capsules filled with PCM having different melting points. Energy Build 2014;68:639–46.
[47] Xu JZ, Gao BZ, Kang FY. A reconstruction of Maxwell model for effective thermal conductivity of composite materials. Appl Therm Eng 2016;102:972–9.